ANL/CMT/CP-97833

CHARACTERIZATION OF PHASE ASSEMBLAGE AND DISTRIBUTION IN TITANATE CERAMICS WITH SEM/EDS AND X-RAY MAPPING#

J.S. Luo, V.N. Zyryanov, A. Bakel, and D. Chamberlain
Argonne National Laboratory, Argonne, IL 60439

June1999
revised

To be published in the Proceedings of the 101st American Ceramic Society Annual Meeting, April 25-29, 1999, Indianapolis, IN

#The work at ANL was sponsored by the U.S. Department of Energy (DOE), Fissile Materials Disposition Program (FMD), under Contract W-31-109-ENG-38.

DISCLAIMER

DISCLAIMER

Portions of this document may be illegible in electronic image products. Images are produced from the best available original document.

CHARACTERIZATION OF PHASE ASSEMBLAGE AND DISTRIBUTION IN TITANATE CERAMICS WITH SEM/EDS AND X-RAY MAPPING

J.S. Luo, V.N. Zyryanov, A.J. Bakel, and D.B. Chamberlain
Argonne National Laboratory, Argonne, IL 60439

ABSTRACT

Titanate ceramics have been selected for the immobilization of excess plutonium. The baseline ceramic formulation leads to a multi-phase assemblage, which consists of a majority pyrochlore phase plus secondary phases. The phase distribution depends on processing conditions and impurity loading. In this paper, we report on the characterization of the phase assemblage and distribution in titanate ceramics using scanning electron microscopy (SEM), energy dispersive x-ray spectroscopy (EDS), and x-ray dot mapping. Two titanate ceramics were studied: a baseline ceramic and a ceramic with impurities. In the baseline ceramic, the secondary phases that were observed include zirconolite, brannerite, and rutile. Additional phases, such as perovskite, an Al-Ti-Ca phase, and a silicate phase, formed in the impurity ceramic. The distribution of these phases was characterized with backscattered electron (BSE) imaging, except for zirconolite. While the zirconolite exhibited weak contrasts in BSE images and could not be easily distinguished from the pyrochlore matrix, its distribution was effectively characterized with x-ray mapping. Quantitative analyses of BSE images and x-ray maps reveal that the impurity ceramic contains less brannerite, rutile, and pores than the baseline ceramic.

INTRODUCTION

Titanate-based ceramics have been selected for the immobilization of excess weapons plutonium.[1] Corrosion tests are being conducted at Argonne National Laboratory to evaluate the behavior of the matereials.[2] The chemistry and distribution of the phases, including minor phases, must be understood to meaningfully interpret the corrosion tests. This information can also be utilized to improve the formulation of the ceramic.

The major phases that are present in these titanate ceramics may include pyrochlore, zirconolite, and brannerite, depending on the formulation and processing conditions. Other phases that have been previously observed in the ceramic system are rutile, hollandite, and perovskite.[3] It has also been reported that impurities added to the ceramic may affect the phase chemistry and distribution.[2]

Scanning electron microscopy (SEM) coupled with energy dispersive x-ray spectroscopy (EDS) and image analysis is a powerful way to characterize the phase assemblage and distribution in a complex ceramic system.[4] The different phases that may be present in the ceramic can be readily distinguished based on their chemical compositions and subsequently correlated with the corresponding microstructure and morphologies. The spatial distribution of a specific phase may be imaged with x-ray dot mapping of the intensity of the x-ray emitted by the signature element in that phase.

Using a combination of SEM, EDS, and x-ray dot mapping, we investigated two titanate-based ceramics: a baseline ceramic and a ceramic with a large spectrum of impurities added. The purpose of this study was to characterize the microstructure and phase distribution in both ceramics.

EXPERIMENTAL PROCEDURES

Both ceramics were prepared at Lawrence Livermore National Laboratory (LLNL) under similar conditions. The nominal compositions of the two ceramics are listed in Table 1. The two ceramics contain the same composition with regard to the major components (Ti, U, Hf, Ce, Ca, Gd) (see Table 1a), while the impurity ceramic consists of a wide spectrum of components, totaling 7.9 mass % (see Table 1b).

Table 1a. Nominal compositions of major components in baseline and impurity ceramics E (mass %)

	Ti	U	Ca	Hf	Gd	Ce	O[a]
Baseline Ceramic	21.7	21.2	7.2	9.1	6.2	6.2	28.4
Impurity Ceramic	18.6	18.0	7.6	7.8	5.3	5.3	29.5

Table 1b. Nominal compositions of the elements added in the impurity ceramic (mass %)

Si	Al	Fe	Cr	Ni	Mg	Na	K	Mo	Ta	W	F	Cl	B	Total
0.7	1.1	0.4	0.1	0.3	0.5	0.5	0.9	0.4	0.5	0.4	0.6	1.4	0.1	7.9

[a] Oxygen calculated by difference.

The samples for SEM/EDS analyses were polished with diamond paste and examined using either a Topcon ABT-60 or Hitachi 3000N SEM; both are equipped with a BSE detector and a Noran Vantage DI x-ray microanalysis and digital imaging system. The Vantage system, which has an ultra-thin window x-ray detector and digital pulse processor, permits x-ray mapping and EDS on selected areas of samples. The SEM/EDS analyses were done at an accelerating voltage of 20-25 kV with a working distance of 15-20 mm and 0° sample tilt. The backscattered electron mode was employed to enhance the contrasts among different phases. Phases were identified by comparing the acquired EDS spectra with the known compositions based on both the stoichiometries of existing phases and x-ray diffraction identification of the structure. X-ray maps were collected with conventional point dwell methods in which an EDS spectrum is acquired for each

pixel. Regions corresponding to the mapped elements are located in the spectrum and are automatically set up by the Vantage microanalysis system. Each map, composed of a matrix of pixels, views the spatial distribution of a particular element. X-ray maps acquired in this study have resolution a of 1250 x 1250 pixels. Digital image processing and analysis were carried out using the NIH Image program.[5] The phase of interest was selected by setting brightness threshold based on the gray level of the phase. The digital images for different phases were then analyzed by NIH Image to determine the desired parameters, such as area fraction, size distribution, and orientation.

RESULTS AND DISCUSSION

Figure 1a is a BSE image taken on a polished surface of the baseline ceramic. The microstructure shows two secondary phases and pores of 5-10 μm in diameter. The secondary phases can be distinguished in the BSE images based on their different gray levels, which are, in turn, proportional to the average atomic number, Z, of that phase. Brannerite, due to its high U content, exhibits a brighter contrast in a BSE image. Rutile shows a dark gray contrast, and pores are completely black. It should be noted that zirconolite, a possible stable phase in the system, was not distinguishable from the pyrochlore matrix in BSE images because of its similar average atomic number to pyrochlore. In the impurity ceramic, additional secondary phases were observed in the BSE image (Fig. 1b). These phases are perovskite, a silicate phase, and a Ca-Al-Ti phase, whose crystal structure has not been identified. Interestingly, zirconolite can be readily discerned on the basis of its characteristic needle structure,[3] although it remains a gray level nearly identical to that of the pyrochlore matrix.

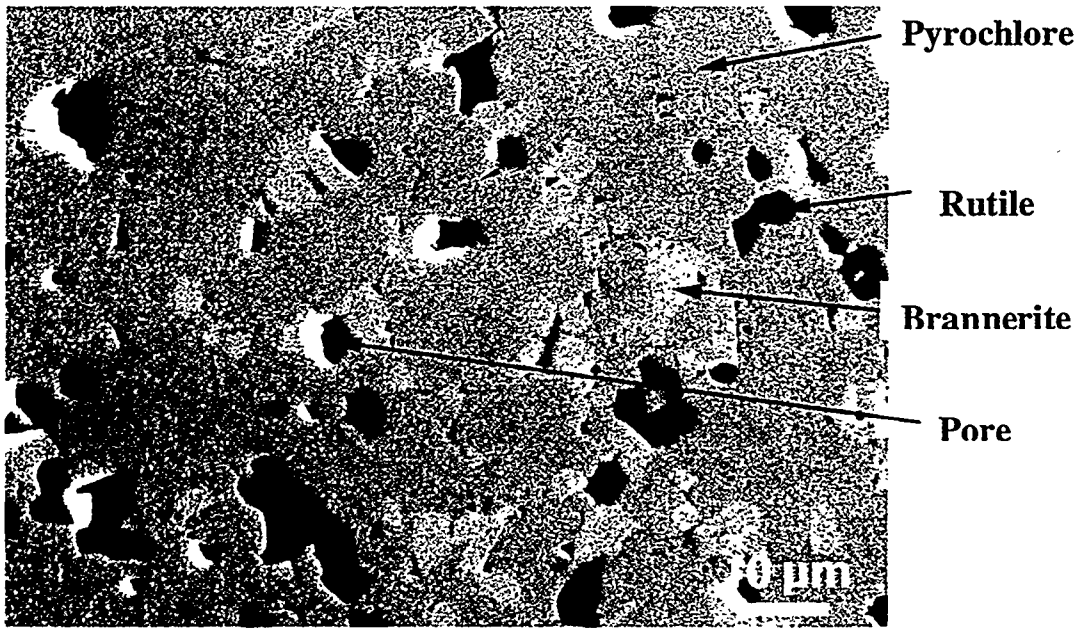

(a)

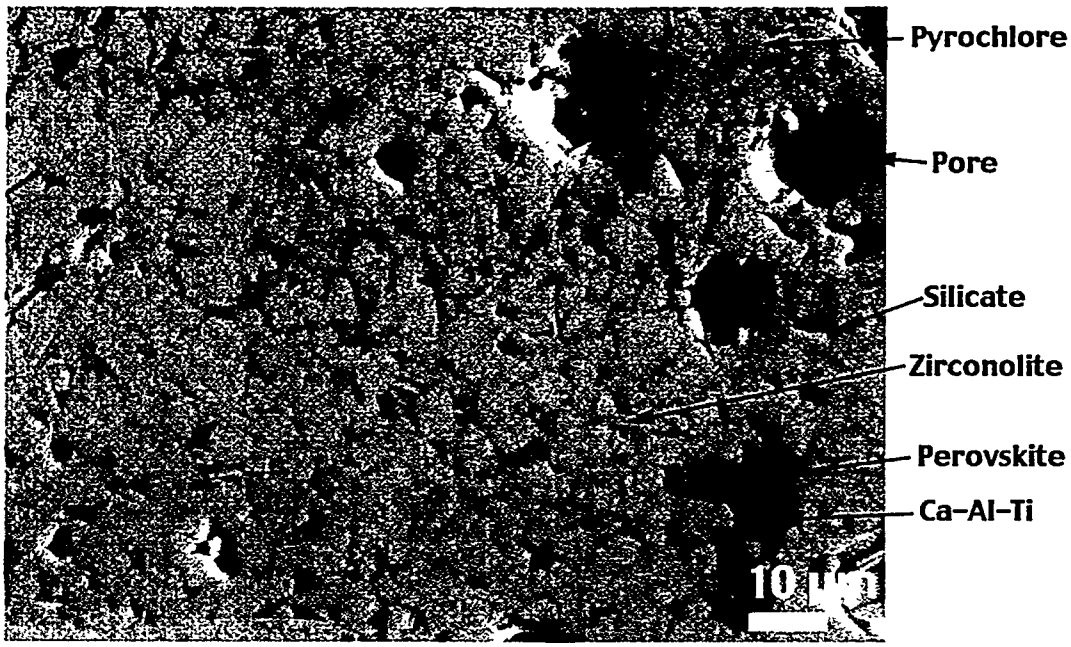

(b)

Fig. 1. Backscattered electron images of (a) the baseline ceramic and (b) the impurity ceramic.

Figure 2 shows the EDS spectra acquired for the four major phases (brannerite, rutile, zirconolite, and pyrochlore) present in the baseline ceramic. Uranium is distributed in all four phases but is enriched in the brannerite phase. Rutile, a Ti-rich phase, also contains small amounts of Hf and U. The major elemets in zirconolite and pyrochlore include Ti, U, Hf, and Ca. However, the distribution of U and Hf is quite different between the two phases: pyrochlore is able to incorporate more U in its structure, whereas Hf tends to segregate in the zirconolite structure. Such composition differences allow these two phases to be differentiated in a Hf x-ray map (where zirconolite would exhibit a brighter contrast) or U x-ray map (where zirconolite would exhibit a darker contrast).

The four phases identified in the baseline ceramic (pyrochlore, zirconolite, brannerite, and rutile) were also found in the impurity ceramic. In addition, the following minor phases were found: perovskite, an Al-Ti-Ca-O phase, and a silicate phase. The Al-Ti-Ca-O phase is Al-rich but also contains some Ca and Ti (Fig. 3a). This phase was often segregated and formed large grains in the impurity ceramic (see Fig. 1b). The crystal structure of the Al-Ti-Ca-O phase has not been identified. The silicate phase seems to be a glassy phase which contains a large mix of the impurity elements. The relative ratios of various elements in the phase vary significantly from one area to another, suggesting a non-stiochiometric composition. Typically, this phase contains large amounts of Si-Al-Mg-P, in additional to U, Ti, Ca, and Ce (see Fig. 3b).

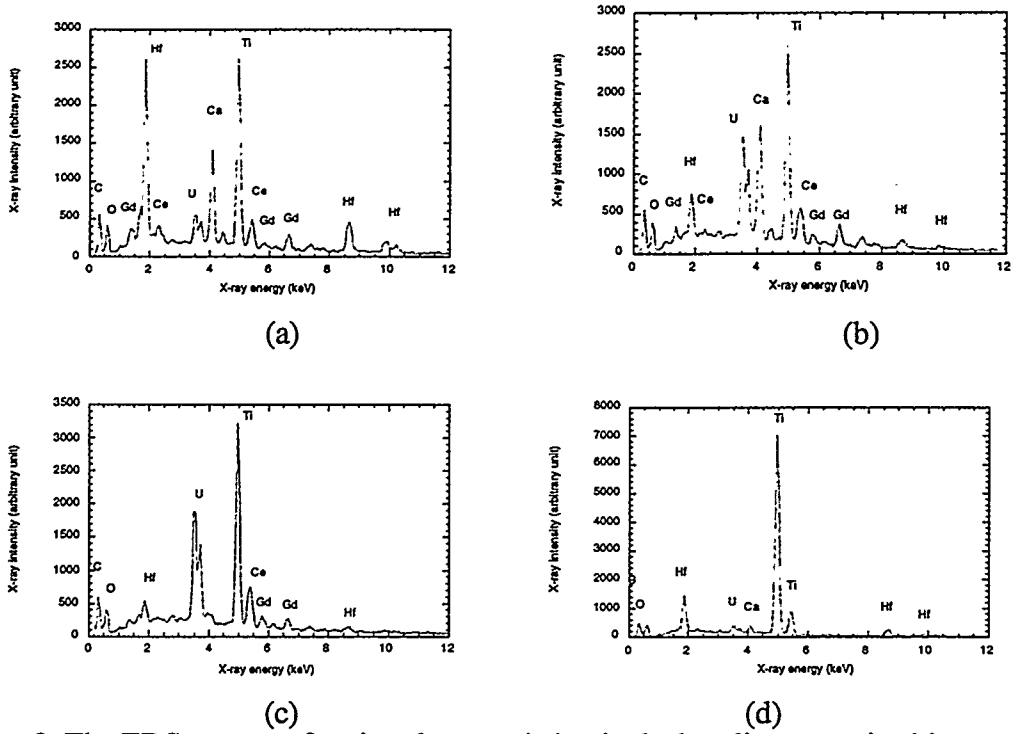

Fig. 2. The EDS spectra of major phases existing in the baseline ceramic: (a) pyrochlore, (b) zirconolite, (c) brannerite, and (d) rutile.

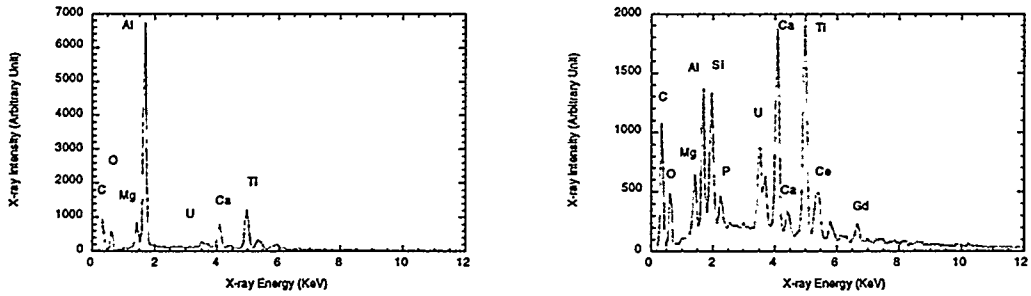

Fig. 3. The EDS spectra of (a) Al-Ti-Ca-O phase and (b) silicate glassy phase.

Figure 4 shows the x-ray maps obtained for U, Hf, and Ti in the baseline ceramic, together with a backscattered electron image that was taken in the same area. The presence of a large quantity of the zirconolite phase in the sample can be clearly seen, whereas it is not evident in the BSE image. Because U is depleted and Hf enriched in zirconolite compared with pyrochlore, zirconolite exhibits a dark contrast on a U map but a bright contrast on a Hf mapping. It is noted that the

zirconolite is visually easier to distinguish on the Hf map. On the other hand, U and Ti maps show that U is enriched in the brannerite phase, and Ti is enriched in rutile, respectively.

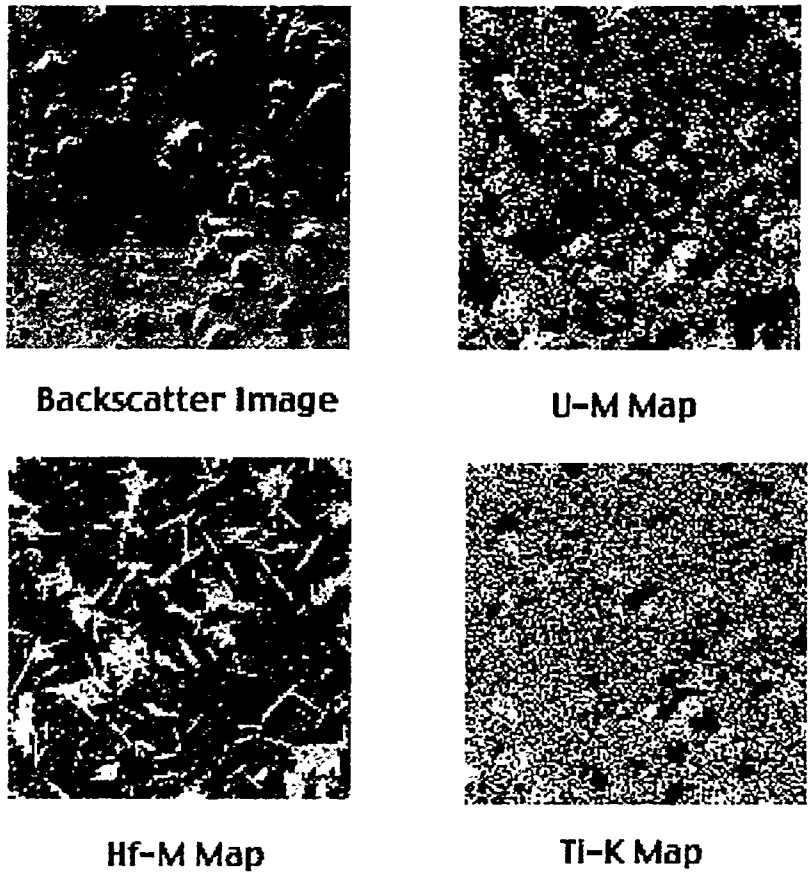

Fig. 4. Backscattered electron image and x-ray maps with U-M, Hf-M, and Ti-K of the baseline ceramic. The white contrasts in the U, Hf and Ti maps correspond to the distribution of brannerite, zirconolite, and rutile, respectively. The contrast for zirconolite in the x-ray map has been dramatically improved over that in the BSE image.

Figure 5 shows the x-ray maps obtained for Hf and Al in the impurity ceramic. The zirconolite phase formed in this sample has a morphology characteristic of needles, as opposed to formation of blocks in the baseline ceramic (see Fig. 4). The Al map confirms the inhomogeneous distribution of the Al-Ti-Ca-O phase, consistent with the BSE observation that this phase tends to segregate into large grains.

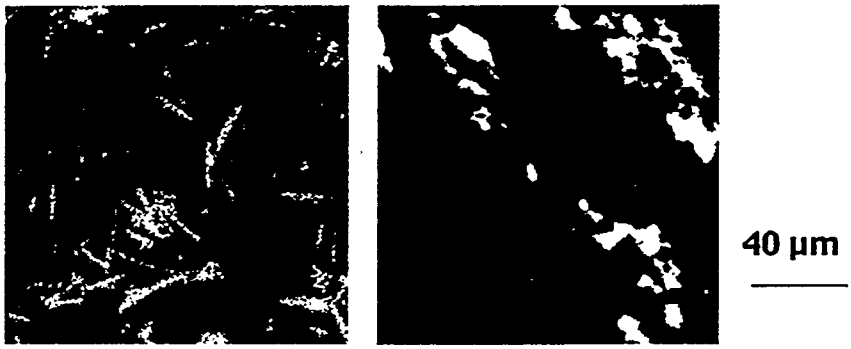

Fig. 5. The x-ray maps of Hf-M and Al-K for the impurity ceramic.

Table 2 compares the area fractions of pores and secondary phases existing in the baseline ceramic and the impurity ceramic. Area fractions of phases were obtained with image analysis of x-ray maps, and area fractions of pores were obtained with image analysis of SEM images. Compared with the baseline ceramic, the impurity ceramic has a lower area fraction of pores and a very small amount of rutile and brannerite phases.

The porosity in the baseline measured with image analysis is very close to that calculated by comparing the geometric density with the theoretical density (about 80 %). This provides some confidence in the application of image analysis in these ceramics. It should be pointed out that the image analysis technique may not be suitable to quantify a minor but segregated phase such as the Al-Ti-Ca-O phase because the results are not necessarily representative. For example, the area fraction of the Al-rich phase is as high as 14 % based on the image analysis of the Al map in Figure 5, and is not representative of its true fraction in the whole ceramic.

Table 2. Area fractions of pores and secondary phases in titanate ceramics.

	Pores	Zirconolite	Rutile	Brannerite
Baseline	21%	21.%	6.9%	13%
Impurity	11%	17%	<1 %[a]	<1 %[a]

[a] These phases are small scattered particles and may not be effectively quantified with image analysis.

CONCLUSIONS

We have conducted detailed microstructural characterization of both the baseline and impurity ceramic using SEM/EDS, x-ray mapping, and image analysis. In the baseline ceramic, the secondary phases that were observed include zirconolite, brannerite, and rutile. Additional phases, such as perovskite, an Al-Ti-

Ca phase, and a silicate phase, formed in the impurity ceramic. The distribution of the phases was characterized with backscattered electron (BSE) imaging. However, the zirconolite phase exhibits a very weak contrast in the BSE image and can only be effectively imaged with x-ray mapping. Quantitative analyses of BSE images and x-ray maps indicate that the impurity ceramic contains less brannerite, rutile, and pores compared with the baseline ceramic.

ACKNOWLEDGMENT

The authors thank Dr. E. Buck and Mr. M. Hash for their critical reading of the manuscript and J. Harmon for his editorial assistance. The work at ANL was sponsored by the U.S. Department of Energy (DOE), Fissile Materials Disposition Program (FMD), under Contract W-31-109-ENG-38.

REFERENCES

[1]S.G. Cochran, W.H. Danker, T.A. Edmunds, L.M. MacLean, and T.H. Gould, *Fissile Materials Disposition Program Final Immobilization Form Assessment and Recommendation*, UCRL-ID-128705, Lawrence Livermore National Laboratory, Livermore, CA (1997).

[2]A.J. Bakel, V.N. Zyryanov, C.J. Mertz, E.C. Buck, D.B. Chamberlain, "Corrosion behavior of pyrochlore-rich titanate ceramics for plutonium disposition; impurity effects," To be published in the Proceedings of the 1998 Fall Meeting of the Materials Research Society Nov 30 - Dec 4, 1998 Boston, MA.

[3]E.C. Buck, E. Ebbinghaus, A.J. Bakel, and J.K. Bates, "Characterization of a plutonium-bearing zirconlite-rich ceramic," Mat. Res. Soc. Symp. Proc. **465**, pp.1259-1266 (1997).

[4]J.S. Luo, N. Merchant, E.J. Escorcia-Aparicio, V.A. Maroni, and B.S. Tani, "Composition and microstructural evolution of nonsuperconducting phases in silver-clad $(Bi,Pb)_2Sr_2Ca_2Cu_3O_x$ composite conductors," *J. Mater. Res.* **9**, pp. 3059-3067 (1994).

[4]NIH Image, Version 1.61, Wayne Rasband, author, National Institute of Health, Washington, DC.